

Measuring Kerrness in Binary Black Hole Simulation Ringdowns

Final Report

LIGO SURF Program, Summer 2016

LIGO Document T1600279

Nicholas Meyer,¹ Maria Okounkova,¹ and Mark A. Scheel¹

¹*Theoretical Astrophysics 350-17, California Institute of Technology, Pasadena, CA 91125, USA*

(Dated: September 23, 2016)

After a single black hole forms from the merger of a black hole binary, it enters the ringdown phase, radiating away energy in gravitational waves until it settles into a stationary Kerr black hole. However, the point at which the resultant spacetime becomes close to Kerr has not yet been established. Furthermore, how close to the merger phase in a gravitational waveform can LIGO apply data analysis techniques that assume that the remnant black hole is Kerr (or a perturbation thereof)? In order to address these questions, it is helpful to consider local quantities which measure the similarity of a spacetime to Kerr. We evaluate several local measures of “Kerrness” on volume data from the ringdown phase of a binary black hole simulation of the GW150914 event using the Spectral Einstein Code (SpEC). We also evaluate these quantities on single (Kerr) black hole simulations for validation.

NUMERICAL RELATIVITY AND KERRNESS BACKGROUND

The first detection of gravitational waves originating from a binary black hole merger [1] has provided a significant confirmation of the predictions of general relativity and has opened the door to many more such tests and observations of black holes. Numerical relativity is the field which concerns the simulation and evolution of spacetimes by solving Einstein’s equations. Its role in LIGO includes correlating observed gravitational waveforms with the local properties of their sources [10].

Theoretical work on binary black hole mergers and LIGO data analysis techniques may

assume a perturbed Kerr spacetime during ringdown [2, 3]. Although simulations have been run which show that the remnant spacetime resulting from a binary black hole merger is a Kerr black hole at the final moment of the simulation [7, 9], the point at which the assumption of a perturbed Kerr spacetime becomes valid has not been established in previous analysis.

The project concerns the evaluation of measures of “Kerrness”, or similarity to the Kerr spacetime, including the speciality index \mathcal{S} [4] and the more recently proposed \mathcal{L} by García-Parrado [5]. The goal is both to validate that these are appropriate measures of Kerrness through simulations and to use them to more quantitatively define when a remnant spacetime can be considered adequately close to Kerr.

These invariant measurements are first validated on a single (Kerr) black hole simulation; the observation of sensible behavior on the single black hole simulation serves both to validate the theory itself and that the terms have been implemented correctly in the code. After this validation, the quantities are computed on the ringdown phase of a simulation of the GW150914 binary black hole merger.

$$S = \frac{27J^2}{I^3} \quad (1)$$

FIG. 1: Definition for the speciality index [4]. This quantity is 1 for a Kerr spacetime.

$$\mathcal{L} \equiv \frac{(\mathbf{r}(A) + \mathbf{r}(B))^2 + (\mathbf{j}(A)_i + \mathbf{j}(B)_i)(\mathbf{j}(A)^i + \mathbf{j}(B)^i) + (\mathbf{t}(A)_{ij} + \mathbf{t}(B)_{ij})(\mathbf{t}(A)^{ij} + \mathbf{t}(B)^{ij})}{\sigma^{14}} + \frac{\mathbf{a}_{ij}\mathbf{a}^{ij} + \mathbf{b}_{ij}\mathbf{b}^{ij}}{\sigma^4} + \frac{((1 - 3\lambda^2)\beta + \lambda(3 - \lambda^2)\alpha)^2}{\sigma^2} + \frac{(\mathfrak{B}_{ij}\mathfrak{B}^{ij})^3}{\sigma^4} + \frac{(\mathfrak{C}_{ij}\mathfrak{C}^{ij})^3}{\sigma^7} + \frac{\Omega}{\sigma^2} \quad (2)$$

FIG. 2: Positive Kerrness invariant proposed by García-Parrado [5]. This quantity vanishes at every point for a Kerr spacetime, and is being investigated as a measurement of Kerrness. Compute items for the first three terms have been created and computed on single black hole simulations. Each tensor and scalar quantity presented in the equation is defined in terms of contractions of the electric and magnetic components of the Weyl tensor.

MOTIVATION FOR CHOICE OF KERRNESS QUANTITIES

Speciality Index: S

The speciality index, already implemented in SpEC, was a logical choice to run as an exercise; when setting up simulations it was possible to test and eliminate errors relating to this set up using the speciality index so that errors when running the simulations on \mathcal{L} could be known to lie in the implementation of \mathcal{L} in SpEC.

The speciality index is a complex quantity which is 1 for an algebraically special spacetime [4], and so in a numerical simulation of a Kerr spacetime, the real part should converge to 1 and the imaginary part to 0.

The quantity \mathcal{L} is a non-negative quantity which vanishes for a Kerr spacetime [5]. Furthermore, it can be decomposed into six non-negative terms, each of which independently vanish under this condition [5]. The first three terms of this quantity were implemented in SpEC.

\mathcal{L} more specifically measures Kerrness than \mathcal{S} does because \mathcal{L} vanishes for Kerr rather than for a strict superset thereof [4, 5].

SpEC simulations consist of evolving “slices” (3 dimensional spatial hypersurfaces) through time [8]. The computation of \mathcal{L} involves four-dimensional tensors, but because this quantity can be equivalently computed using pulled-back tensor quantities to a spatial hypersurface [5], it can be computed on each slice (hence the Latin indices in FIG. 2). This makes the implementation in SpEC much simpler, since many subroutines which can be used in computing \mathcal{L} are spatial. In addition, analysis of behavior with respect to time is simpler with a quantity computed on each slice.

VALIDATION OF \mathcal{L} AND \mathcal{S} ON SINGLE BLACK HOLE SIMULATIONS

The quantity \mathcal{S} is equal to 1 for an algebraically special spacetime, which encompasses Kerr [4].

The quantity \mathcal{L} vanishes at all points given a Kerr spacetime [5], in which case the following conditions hold [5]:

1. $\mathbf{r}(A) = -\mathbf{r}(B)$
2. $\mathbf{j}(A)_i = -\mathbf{j}(B)_i$
3. $\mathbf{t}(A)_{ij} = -\mathbf{t}(B)_{ij}$
4. $\mathbf{a}_{ij} = 0$
5. $\mathbf{b}_{ij} = 0$
6. $((1 - 3\lambda^2)\beta + \lambda(3 - \lambda^2)\alpha) = 0$

7. $\mathfrak{B}_{ij} = 0$

8. $\mathfrak{C}_{ij} = 0$

9. $\Omega = 0$

In order to validate the theoretical behavior of \mathcal{S} and the first six conditions for \mathcal{L} , \mathcal{S} and the first three terms of \mathcal{L} were computed on a simulation of a single (Kerr) black hole at several resolutions.

Random Spin Vector

Initial implementation of \mathcal{L} in SpEC validated the results on a single black hole simulation with a spin vector fixed in the z direction. Because it is theoretically possible that bugs may exist in the code which do not affect such spin vectors, the following Perl code was used to generate a dimensionless spin vector with magnitude between zero and 0.9 and a random direction:

```
$PI      = 3.14159265358979;  
  
$r       = rand() * 0.9;  
$phi     = rand() * 2 * $PI;  
$theta   = rand() * $PI;  
$x       = $r * sin($theta) * cos($phi);  
$y       = $r * sin($theta) * sin($phi);  
$z       = $r * cos($theta);
```

where $\$x$, $\$y$, $\$z$ represent the x, y, and z components of the dimensionless spin vector. When simulations at several numerical resolutions were run to generate convergence plots, the same spin vector was used for each of the resolutions.

Convergence behavior was observed to be the same with several arbitrary randomly generated spin vectors as with a spin vector pointed along the z-axis with magnitude 0.4 (used in the convergence plots here).

Convergence of \mathcal{S} to theoretical value

In FIG. 3, convergence of the absolute errors of the real and imaginary parts of \mathcal{S} can be seen with respect to resolution (increased resolution entails the simultaneous increase in both angular resolution and timestep resolution). Exponential convergence can be observed.

In FIG. 4, the stability of the errors with respect to time validates the numerics of the simulation.

Convergence of \mathcal{L} quantities to theoretical values

In FIG. 5, exponential convergence of the first three terms of \mathcal{L} can be seen.

FIG. 6 demonstrates the time stability of the numerics using a time plot of the third term.

Note that because absolute errors are being plotted here, the multiplicative or “vertical” difference between the convergence of \mathcal{S} and \mathcal{L} is not meaningful.

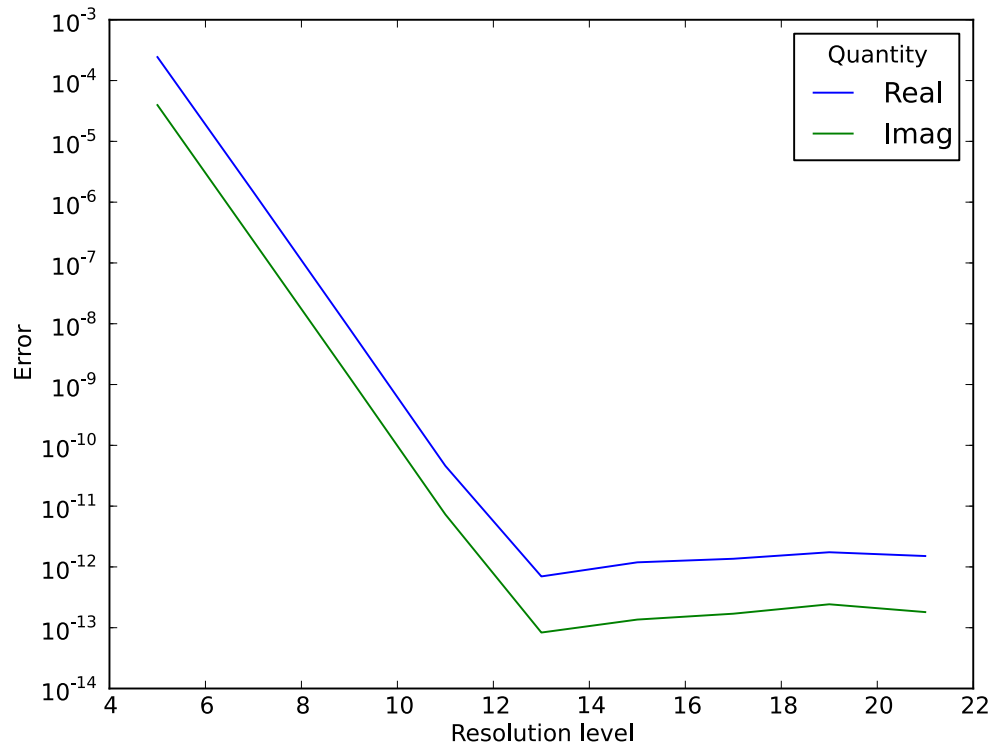


FIG. 3: Absolute error of the real and imaginary parts of \mathcal{S} with respect to resolution. As the plot is with a logarithmic y-axis, the exponential convergence manifests in a straight line with negative slope, eventually flattening out when a numerical noise floor is reached.

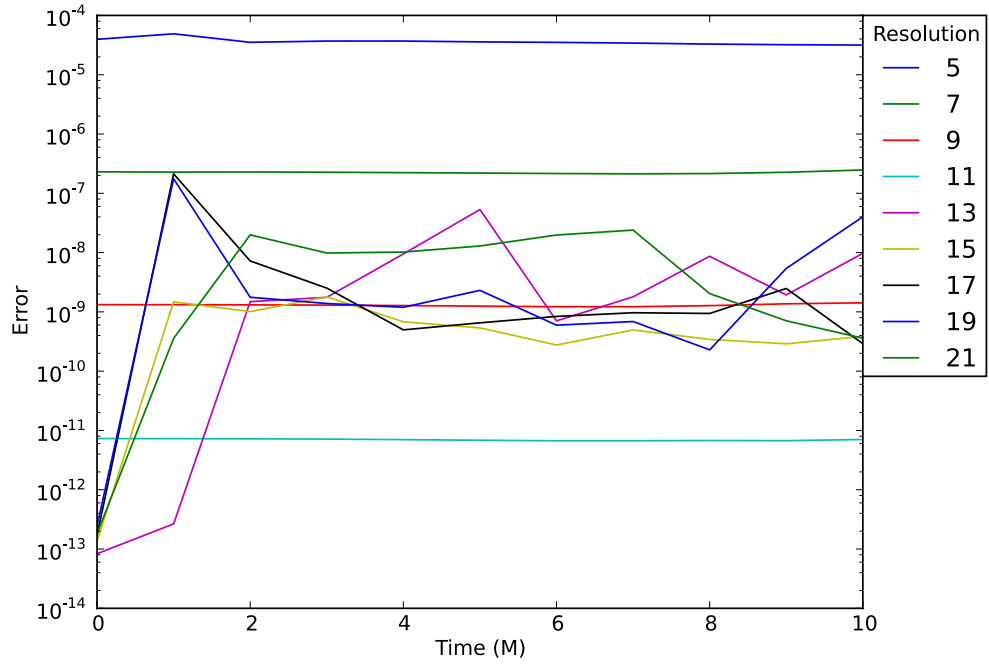
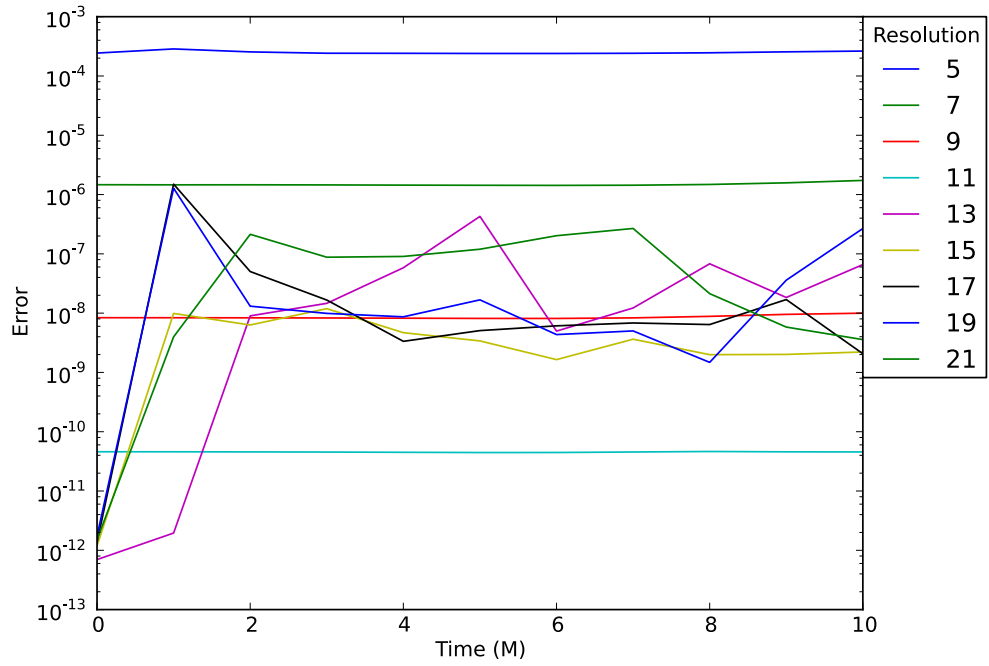


FIG. 4: Error with respect to time for both the real (top) and imaginary (bottom) parts of S .

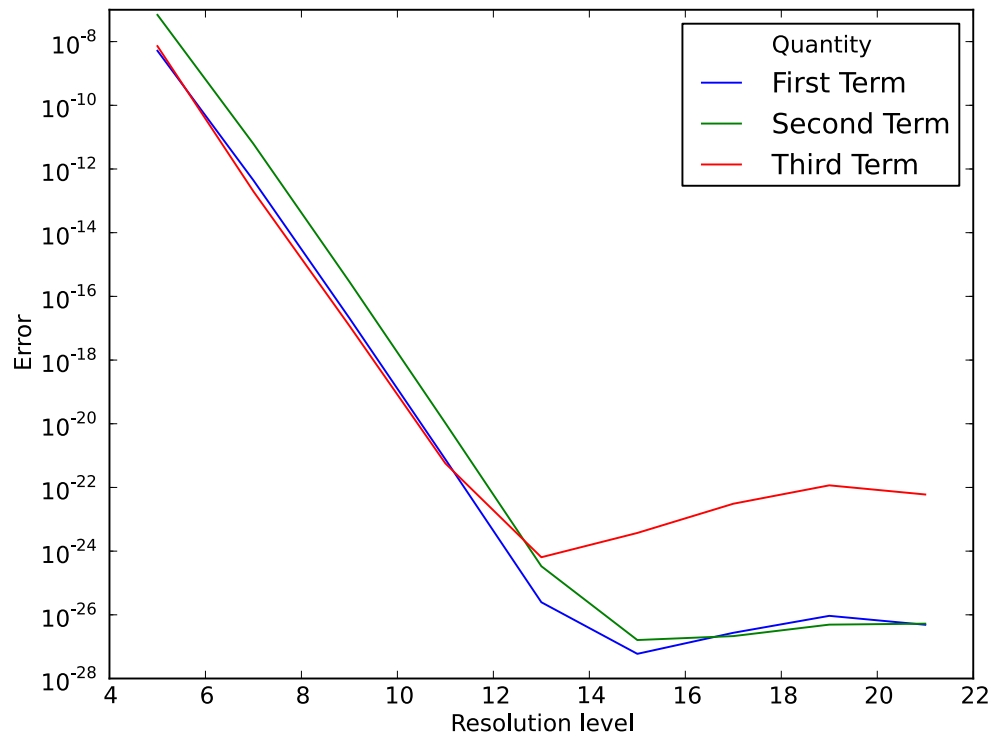


FIG. 5: Absolute error of the first three terms of \mathcal{L} with respect to resolution. Exponential convergence can be seen here as well.

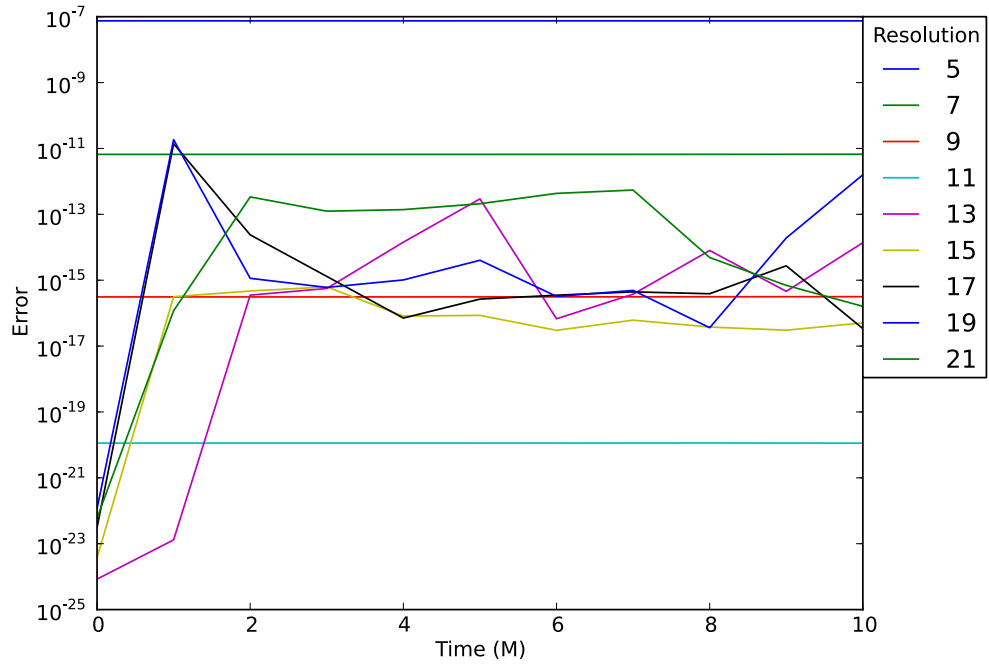


FIG. 6: Error with respect to time of the third term of \mathcal{L} .

\mathcal{S} AND \mathcal{L} ON RINGDOWN OF GW150914 BINARY BLACK HOLE MERGER SIMULATION

Using volume data from the ringdown phase of the GW150914 simulation, plots of the behavior of \mathcal{S} and \mathcal{L} with respect to radius and time were generated.

In FIG. 7-8, plotted is the behavior of the real and imaginary parts of \mathcal{S} and the first three terms of \mathcal{L} with respect to time. The absolute error of each quantity was taken to be the integral of the square of the quantity along the surface of a sphere located at 20 M from the origin (normalized by the area of the sphere). For the real part of \mathcal{S} , the error is the absolute difference between this value and 1.

With \mathcal{L} in particular, the values can be seen to approach what would be expected for a Kerr spacetime as time progresses.

In FIG. 9-10, the errors are plotted with respect to time at 80 M from the origin. A settling to zero (or 1 in the case of the real part of \mathcal{S}) as time progresses is also observed, after an initial upward spike of many orders of magnitude.

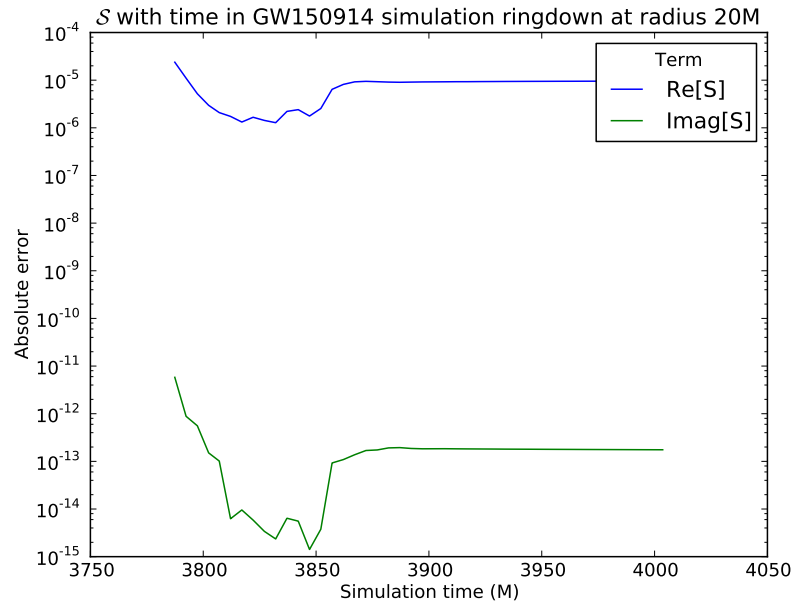


FIG. 7: Behavior of the real and imaginary parts of \mathcal{S} with respect to time at 20M from the origin.

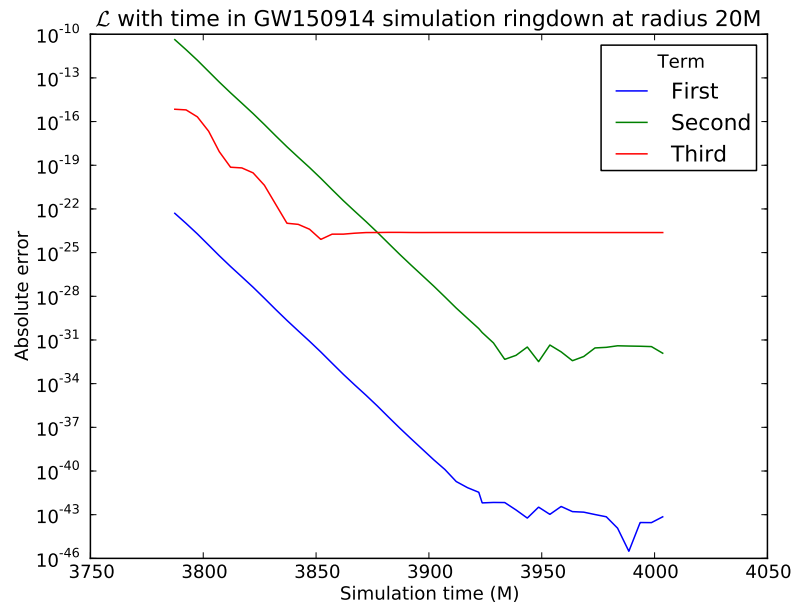


FIG. 8: Behavior of the first three terms of \mathcal{L} with respect to time at 20M from the origin.

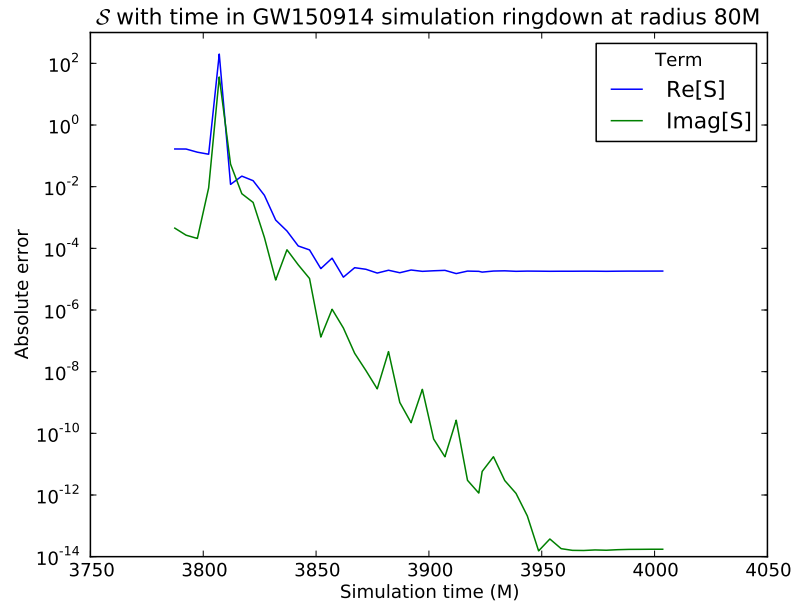


FIG. 9: Behavior of the real and imaginary parts of \mathcal{S} with respect to time at 80M from the origin.

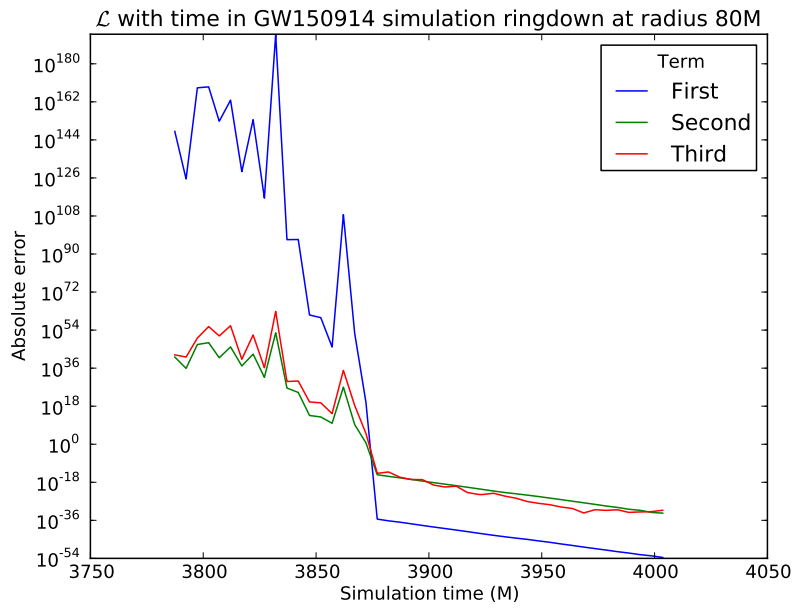


FIG. 10: Behavior of the first three terms of \mathcal{L} with respect to time at 80M from the origin.

NORMALIZATION OF TENSOR AND SCALAR QUANTITIES

When computing the quantities measuring Kerrness on the single black hole, deviations from their theoretical values are a form of absolute error, which has been shown to converge exponentially with increasing angular resolution (see FIG. 3, 5). In order to more meaningfully examine these errors, strategies for normalizing the errors were investigated. As most of the quantities considered vanish for a Kerr spacetime, exactly what constitutes a relative error is somewhat nontrivial and care must be taken to define error normalization.

Consider the quantity

$$E_{ij} = \sum_{k=0}^n F_{ij}^k \quad (3)$$

where E_{ij} is a tensor quantity which vanishes analytically and F_{ij}^k , $0 \leq k \leq n$ are tensors which do not independently vanish analytically. The **local normalization** of E_{ij} , which defines the relative error due to numerics in the single black hole simulation, is given by

$$\hat{E}_{ij} = \frac{E_{ij}}{\sqrt{\sum_{k=0}^n F_{ij}^k F_k^{ij}}} \quad (4)$$

The normalization for tensors of ranks other than two and for scalar quantities is similarly defined as the quotient of the quantity and the square root of the sum of the products of each tensor F with all indices lowered and with all indices raised (i.e. $\sum_{k=0}^n F_i F^i$ and $\sum_{k=0}^n F^2$).

Alternatively, the **global normalization** of the quantity E_{ij} is given by

$$\frac{L_2(E_{ij})}{L_2\left(\sqrt{\sum_{k=0}^n F_{ij}^k F_k^{ij}}\right)} \quad (5)$$

where the L_2 norm of a quantity x indexed as x_i with respect to theoretical value \tilde{x} is given by

$$L_2(x) = \sqrt{\sum_i^N \frac{(x_i - \tilde{x})^2}{N}} \quad (6)$$

Global normalization proves to be a more useful quantity to analyze since locally normalized quantities can blow up in certain regions where the quantity nearly vanishes. Analysis of normalized quantities is ongoing.

MINOR CORRECTION TO GARCÍA PARRADO 2015 [5]

A consistency check between evaluation of the expression for the intermediate quantity Θ^{\parallel} [5] between equation (7) (equation (66) [5])

$$\Theta^{\parallel} = \frac{1}{A^2 + B^2} \left((2B(E^{\beta\alpha}E^{\gamma}_{\alpha} - B^{\beta\alpha}B^{\gamma}_{\alpha}) + 4AB^{\beta\alpha}E^{\gamma}_{\alpha})K_{\beta\gamma} - \frac{2}{3}\varepsilon_{\beta\gamma\delta}(E^{\alpha\beta}(BD^{\delta}B_{\alpha}{}^{\gamma} + AD^{\delta}E_{\alpha}{}^{\gamma}) + B^{\alpha\beta}(-AD^{\delta}B_{\alpha}{}^{\gamma} + BD^{\delta}E_{\alpha}{}^{\gamma})) \right) \quad (7)$$

and equation (8) (equation (71) [5]) in the proof

$$\Theta^{\parallel} \equiv \frac{1}{3}(A^2 + B^2)^{-1}(A\mathcal{L}_{\bar{n}}B - B\mathcal{L}_{\bar{n}}A) \quad (8)$$

yielded different results as summarized in FIG. 11 (a). The cause of this inconsistency was found to be a sign error in one of the terms in equation (66) as described below:

From equation (71)[5],

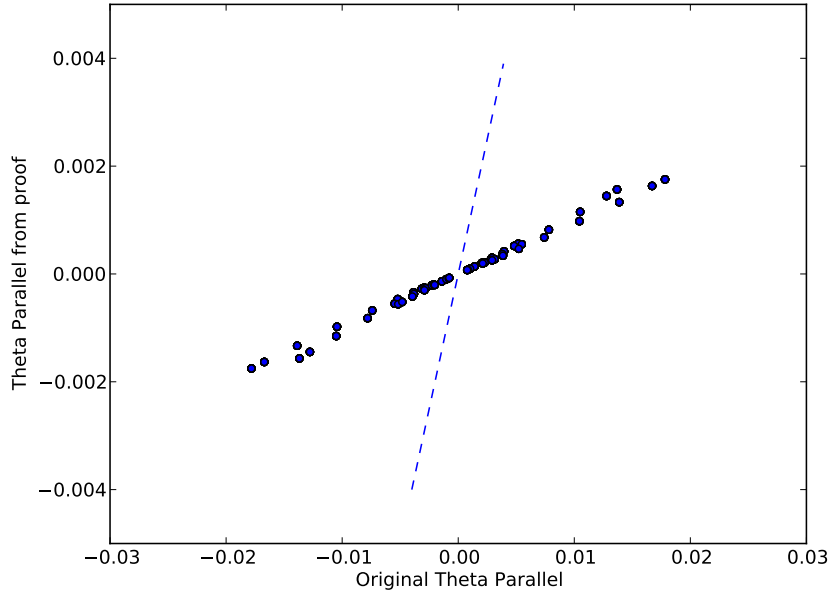
$$\Theta^{\parallel} = \frac{1}{3}(A^2 + B^2)^{-1}(A\mathcal{L}_{\bar{n}}B - B\mathcal{L}_{\bar{n}}A) \quad (9)$$

where $\mathcal{L}_{\bar{n}}A$, $\mathcal{L}_{\bar{n}}B$ are given in (57) and (58)[5]

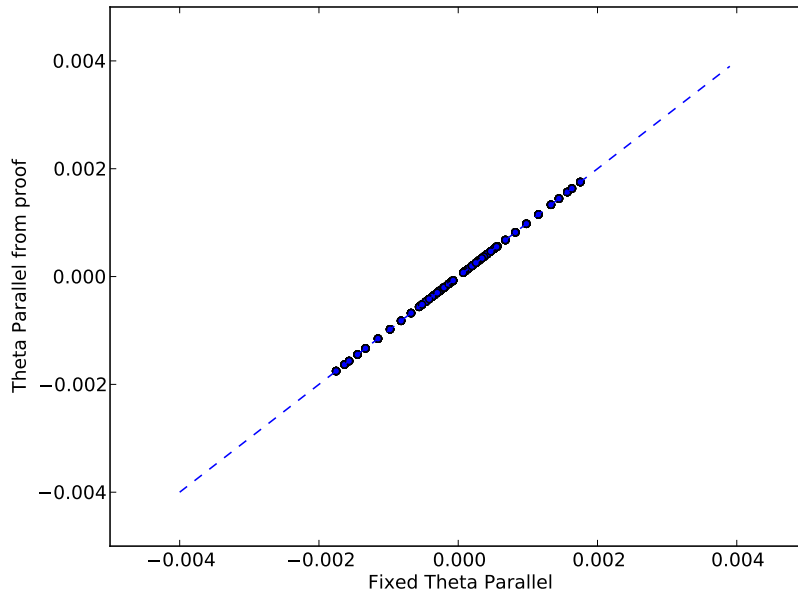
$$\mathcal{L}_{\bar{n}}A = 6(B_{\alpha}{}^{\gamma}B^{\alpha\beta} - E_{\alpha}{}^{\gamma}E^{\alpha\beta})K_{\beta\gamma} + 4AK^{\gamma}_{\gamma} + 2\varepsilon_{\beta\gamma\delta}(E^{\alpha\beta}D^{\delta}B_{\alpha}{}^{\gamma} + B^{\alpha\beta}D^{\delta}E_{\alpha}{}^{\gamma}) \quad (10)$$

$$\mathcal{L}_{\bar{n}}B = -4(3B^{\alpha\beta}E_{\alpha}{}^{\gamma}K_{\beta\gamma} - BK^{\gamma}_{\gamma}) + 2\varepsilon_{\beta\gamma\delta}(B^{\alpha\beta}D^{\delta}B_{\alpha}{}^{\gamma} - E^{\alpha\beta}D^{\delta}E_{\alpha}{}^{\gamma}) \quad (11)$$

Simplifying the result in equation (12) (sign difference from eq. (66)[5] highlighted)



(a)



(b)

FIG. 11: Scatter plots of the original (a) and fixed (b) Θ^{\parallel} quantities against the quantity from the proof for Sphere 1 (6M radius). Because the values for Θ^{\parallel} are analytically identical to one another, the scatter plot points should lie on the dashed line along $y = x$.

$$\begin{aligned}
\Theta^{\parallel} &= \frac{1}{3} (A^2 + B^2)^{-1} \left(-12AB^{\alpha\beta} E_{\alpha}^{\gamma} K_{\beta\gamma} + 4ABK^{\gamma}_{\gamma} + 2A\epsilon_{\beta\gamma\delta} (B^{\alpha\beta} D^{\delta} B_{\alpha}^{\gamma} - E^{\alpha\beta} D^{\delta} E_{\alpha}^{\gamma}) \right. \\
&\quad \left. - 6B(B_{\alpha}^{\gamma} B^{\alpha\beta} - E_{\alpha}^{\gamma} E^{\alpha\beta}) K_{\beta\gamma} - 4ABK^{\gamma}_{\gamma} - 2B\epsilon_{\beta\gamma\delta} (E^{\alpha\beta} D^{\delta} B_{\alpha}^{\gamma} + B^{\alpha\beta} D^{\delta} E_{\alpha}^{\gamma}) \right) \\
&= (A^2 + B^2)^{-1} \left((2B(E_{\alpha}^{\gamma} E^{\alpha\beta} - B_{\alpha}^{\gamma} B^{\alpha\beta}) - 4AB^{\alpha\beta} E_{\alpha}^{\gamma}) K_{\beta\gamma} \right. \\
&\quad \left. - \frac{2}{3} \epsilon_{\beta\gamma\delta} (E^{\alpha\beta} (BD^{\delta} B_{\alpha}^{\gamma} + AD^{\delta} E_{\alpha}^{\gamma}) + B^{\alpha\beta} (BD^{\delta} E_{\alpha}^{\gamma} - AD^{\delta} B_{\alpha}^{\gamma})) \right)
\end{aligned} \tag{12}$$

Note that due to the symmetries of the Electric and Magnetic Weyl tensors E_{ij} and B_{ij} , $B^{\alpha\beta} E_{\alpha}^{\gamma}$ is equivalent to $B^{\beta\alpha} E^{\gamma}_{\alpha}$, and similarly for other seemingly index-swapped terms.

FUTURE WORK

Short term goals

This work can be extended by finishing the implementation of the remaining terms of \mathcal{L} , which are currently non-convergent for reasons assumed to be related to subtle implementation mistakes. It is possible that the cause may be instead be subtle theoretical details which causes the theoretical behavior to not apply, and so if convergence does not occur after further debugging, the expression itself may be analyzed.

In addition, completing the implementation of quantity normalization will add greater perspective when analyzing the convergence of quantities which are analytically zero.

A simplified non-negative quantity featured in a more recent paper by García-Parrado which vanishes for a Kerr [6]. Further work may involve comparing the convergence and behavior of quantities from the 2015 and 2016 papers.

Improvements to the efficiency and stability of the code for \mathcal{L} will be important when using this quantity as a component of future projects. Efficiency can be improved by making use of tensor symmetries to reduce the number of loops during contractions. Due to the time constraints of the SURF, this optimization was not implemented because it could potentially make debugging more difficult; with working implementations though, this enhancement is a logical next step.

Long term goals

The observed behavior of \mathcal{S} and the first three terms of \mathcal{L} on the single black hole simulations and on the GW150914 volume data has validated the use of these quantities as measures of Kerrness.

Longer-term research efforts based on this work include the computation of the quantities studied here in a larger variety of binary black hole simulations. Due to the time constraints of SURF, volume data from an existing simulation was used and only a portion of the ringdown was analyzed; future efforts could involve computing the quantities on new binary black hole simulations with different parameters.

Ultimately, the relationship between local features of Kerrness at the merger and the observed gravitational waveform may lead to insights and in turn help improve LIGO data analysis. These results represent a small step toward this greater goal.

ACKNOWLEDGMENTS

Mentors Maria Okounkova and Mark Scheel, as well as Daniel Hemberger and Leo Stein, made this work possible with assistance on questions about the theory, working with SpEC, debugging, and various other topics.

Access to the zwicky computer, located at the California Institute of Technology, was provided by the Center for Advanced Computing Research (CACR).

Volume data for a simulation of the GW150914 event as well as access to the orca computer was provided by California State University, Fullerton.

Funding and organization of the summer programs which made this project possible include the Caltech Student Faculty Programs (SFP), the LIGO SURF program, the LIGO laboratory, and the National Science Foundation (NSF).

-
- [1] B. P. Abbott et al. Observation of gravitational waves from a binary black hole merger. *Phys. Rev. Lett.*, 116:061102, Feb 2016.
- [2] B. P. Abbott et al. Properties of the binary black hole merger GW150914. 2016.
- [3] B. P. Abbott et al. Tests of general relativity with GW150914. 2016.
- [4] J. Baker and M. Campanelli. Making use of geometrical invariants in black hole collisions. *Physical Review D*, 62(12):127501, December 2000.
- [5] A. García-Parrado Gómez-Lobo. Local non-negative initial data scalar characterization of the Kerr solution. *Physical Review D*, 92(12):124053, December 2015.
- [6] A. García-Parrado Gómez-Lobo. Vacuum type d initial data. *ArXiv e-prints*, February 2016.
- [7] D. A. Hemberger, G. Lovelace, T. J. Loredo, L. E. Kidder, M. A. Scheel, B. Szilágyi, N. W. Taylor, and S. A. Teukolsky. Final spin and radiated energy in numerical simulations of binary black holes with equal masses and equal, aligned or antialigned spins. *Physical Review D*, 88(6):064014, September 2013.
- [8] Maria Okounkova. Private Communication, 2016.
- [9] R. Owen. Final remnant of binary black hole mergers: Multipolar analysis. *Physical Review D*, 80(8):084012, October 2009.
- [10] Mark A. Scheel. Numerical relativity. Lecture.